This article may be downloaded for personal use only. Any other use requires prior permission of the author and AIP Publishing. This article appeared in Ng, Jonathan et al.; An improved ten-moment closure for reconnection and instabilities; Physics of Plasmas 27, 082106, 21 August, 2020; https://doi.org/10.1063/5.0012067 and may be found at https://aip.scitation.org/doi/10.1063/5.0012067. Access to this work was provided by the University of Maryland, Baltimore County (UMBC) ScholarWorks@UMBC digital repository on the Maryland Shared Open Access (MD-SOAR) platform.

Please provide feedback

Please support the ScholarWorks@UMBC repository by emailing scholarworks-group@umbc.edu and telling us what having access to this work means to you and why it's important to you. Thank you.

Physics of Plasmas

An improved ten-moment closure for reconnection and instabilities

Cite as: Phys. Plasmas **27**, 082106 (2020); https://doi.org/10.1063/5.0012067
Submitted: 27 April 2020 . Accepted: 28 July 2020 . Published Online: 21 August 2020

Jonathan Ng, A. Hakim, L. Wang, and A. Bhattacharjee

View Online Export Citation CrossMark

ARTICLES YOU MAY BE INTERESTED IN

Fluid and gyrokinetic turbulence in open field-line, helical plasmas
Physics of Plasmas **27**, 082301 (2020); https://doi.org/10.1063/5.0005333

Announcement: The 2019 James Clerk Maxwell Prize for Plasma Physics
Physics of Plasmas **27**, 080201 (2020); https://doi.org/10.1063/5.0020008

Comparison of multi-fluid moment models with particle-in-cell simulations of collisionless magnetic reconnection
Physics of Plasmas **22**, 012108 (2015); https://doi.org/10.1063/1.4906063

© 2020 Author(s).

Physics of Plasmas ARTICLE scitation.org/journal/php

An improved ten-moment closure for reconnection and instabilities

Cite as: Phys. Plasmas **27**, 082106 (2020); doi: 10.1063/5.0012067
Submitted: 27 April 2020 · Accepted: 28 July 2020 ·
Published Online: 21 August 2020

View Online Export Citation CrossMark

Jonathan Ng,[1,2,a)] A. Hakim,[3] L. Wang,[3] and A. Bhattacharjee[1,3,4]

AFFILIATIONS

[1]Department of Astrophysical Sciences, Princeton University, Princeton, New Jersey 08542, USA
[2]Department of Astronomy, University of Maryland, College Park, Maryland 20742, USA
[3]Princeton Plasma Physics Laboratory, Princeton, New Jersey 08543, USA
[4]Princeton Center for Heliophysics, Princeton University, Princeton, New Jersey 08542, USA

[a)]Author to whom correspondence should be addressed: jonng@umd.edu

ABSTRACT

The integration of kinetic effects in fluid models is important for global simulations of Earth's magnetosphere. The use of the two-fluid ten-moment model, which includes the pressure tensor for both species, has had some success in simulating Ganymede and Mercury with a simple closure model. We discuss a heat flux closure which accounts for some limitations of the earlier work while remaining computationally tractable. Comparisons with kinetic simulations for magnetic reconnection and lower-hybrid drift instabilities show good agreement with kinetic results and improvements on previous closure models.

Published under license by AIP Publishing. https://doi.org/10.1063/5.0012067

I. INTRODUCTION

The modeling of large-scale collisionless plasma environments such as magnetospheres is a challenging problem, as it requires the coupling of global features to small-scale physics. Most global models of Earth's magnetosphere use Magnetohydrodynamics (MHD), which treats the plasma as a single conducting fluid.[1–3] While these models can simulate the large spatial and temporal scales involved, they are missing the small-scale kinetic physics.

There are many approaches to adding physical effects beyond MHD in simulation models, such as the inclusion of pressure anisotropy,[4,5] the Hall-current term,[6,7] the use of hybrid codes with kinetic ions and fluid electrons,[8–11] and embedding kinetic boxes within larger-scale fluid simulations.[12,13]

In this paper, we consider the multi-fluid moment model, in which moments of the kinetic equation up to the pressure tensor are evolved. This has been used in local studies of reconnection and instabilities[14–21] as well as global simulations of Ganymede,[22] Mercury,[23] and Uranus.[24] While these studies have had some success in terms of both theoretical results and observational comparisons, the issue of closure (in this case, the form of the heat flux) still remains, both in terms of physical modeling and computational cost. In contrast to earlier studies, which have used a nonlocal Landau-fluid-like closure,[18] which is costly, or a local relaxation to isotropy,[16,17] which has limitations, to approximate kinetic effects, we employ an effective thermal conductivity. This is similar to the approaches used in Refs. 21 and 25, and we perform comparisons with both kinetic simulations and other closure approximations.

The scope of this paper is confined to two test problems which have been studied extensively using two-fluid and kinetic models. We first study magnetic reconnection using the island coalescence geometry. While this is an idealized setup, the merging of flux tubes is an important process for particle acceleration and energy transfer in space and astrophysical plasmas.[26–28] Previous kinetic studies of coalescence have shown that the normalized reconnection rate is affected by the system-size,[29,30] a result which cannot be reproduced by Hall-MHD because of the importance of ion physics. How well the ten-moment model reproduces these kinetic results depends on the closure used—in Refs. 17 and 18, the importance of the ion pressure tensor could only be recovered at small system sizes, while Ref. 21 found good agreement up to large system sizes. We find that we are able to reproduce the kinetic system-size scaling[29] as well the structure of the ion diffusion region in guide-field reconnection.

We then study the lower-hybrid drift instability (LHDI), which is driven by diamagnetic currents in inhomogeneous plasmas.[31] This instability is found at the edge of current sheets in both simulations and observations.[32–34] In the magnetosphere, the LHDI may drive turbulence during magnetopause reconnection,[35,36] and can quicken the onset of reconnection in regimes relevant to magnetotail

Published under license by AIP Publishing

reconnection.[37,38] Prior studies of the LHDI using the ten-moment model show that it is important to retain the ion kinetic effects using the nonlocal closure,[19,20] and we find the heat flux closure in this work is able to reproduce the growth of the LHDI in a current sheet.

This paper is organized as follows: in Sec. II, we discuss the ten-moment equations used in this paper and various closures. Section III describes a study of reconnection using the island coalescence geometry and simulations of the LHDI are discussed in Sec. IV. We summarize the results in Sec. V.

II. FLUID MODEL

The ten-moment equations are derived by taking moments of the kinetic equation

$$\begin{aligned} &\frac{\partial n}{\partial t} + \frac{\partial}{\partial x_j}(nu_j) = 0, \\ &m\frac{\partial}{\partial t}(nu_i) + \frac{\partial \mathcal{P}_{ij}}{\partial x_j} = nq(E_j + \epsilon_{ijk}u_jB_k), \\ &\frac{\partial \mathcal{P}_{ij}}{\partial t} + \frac{\partial \mathcal{Q}_{ijk}}{\partial x_k} = nqu[iE_j] + \frac{q}{m}\epsilon_{[ikl}\mathcal{P}_{kj]}B_l, \end{aligned} \tag{1}$$

where $\mathcal{P}_{ij}$ and $\mathcal{Q}_{ijk}$ are the second and third moments of the distribution function

$$\begin{aligned} \mathcal{P}_{ij} &\equiv m\int v_iv_jfd^3v, \\ \mathcal{Q}_{ijk} &\equiv m\int v_iv_jv_kfd^3v, \end{aligned} \tag{2}$$

and the square brackets denote a sum over permutations of the indices (e.g., $u_{[i}E_{j]} = u_iE_j + u_jE_i$). The third moment tensor $\mathcal{Q}_{ijk}$ can be written in terms of the heat flux tensor $q_{ijk} \equiv m\int(v_i - u_i)(v_j - u_j)\,(v_k - u_k)fd^3v$

$$\mathcal{Q}_{ijk} = q_{ijk} + u_{[i}\mathcal{P}_{jk]} - 2mnu_iu_ju_k. \tag{3}$$

In earlier work, the closure of the equations in the collisionless limit used a three-dimensional extension of the Hammett–Perkins closure,[18] which can be expressed as follows for both electrons and ions:[39]

$$q_{ijk}(\mathbf{x}) = n(\mathbf{x})\hat{q}_{ijk}(\mathbf{x}), \tag{4}$$

where $\hat{q}_{ijk}$ in Fourier space is $\tilde{q}_{ijk}$ and is calculated as

$$\tilde{q}_{ijk} = -i\frac{v_t}{|k|}\chi k_{[i}\tilde{T}_{jk]}. \tag{5}$$

Here, $\tilde{T}_{jk}$ is the Fourier transform of the deviation of the local temperature tensor from the mean. The $1/|k|$ scaling makes this a non-local closure when expressed in real space[40,41] and provides a 1 to 3 pole Padé approximation of various components of the dielectric tensor. The coefficient $\chi = \sqrt{4/9\pi}$ is the best fit value for the diagonal q_{iii} component and reduces to the closure in Refs. 39 and 40 in the 1-D limit. This is an unmagnetized closure (especially relevant to ions in this geometry in which there is no guide field) which approximates linear phase mixing, allowing the wavenumber-dependent damping of spurious short-wavelength oscillations which are present in higher moment fluid models.[40,42]

The evaluation of the nonlocal closure is computationally expensive due to the need to take the Fourier transform, which scales as $O(N\log N)$ and requires global communications in parallel systems, at every time step. This makes it unsuitable for large scale simulations. Although our previous work used the nonlocal method with improvements in the results,[18] the computational cost was much greater than when using the simpler closure of Refs. 16 and 17, which relaxes the pressure tensor to local isotropy.

In this work, we use an approximation similar to that of Sharma *et al.*,[25] which replaces the nonlocal heat flux with a local heat flux by picking a characteristic wavenumber in Eq. (5). This is equivalent to using a thermal conductivity and was used in studies of fluid simulations of the magnetorotational instability.[25] The resulting expression is

$$q_{ijk} = -\frac{v_t}{|k_s|}\chi\partial_{[i}T_{jk]}, \tag{6}$$

where k_s is a constant or spatially varying parameter for each species. In comparison to Refs. 16, 17, 43, and 44 in which $\partial_i q_{ijk}$ is replaced by a relaxation term proportional to $(P_{ij} - \frac{1}{3}\mathrm{trace}(P)\delta_{ij})$, this provides a local approximation to the heat flux rather than just an isotropization.

Heuristically, the closure is obtained by replacing the $|k|$ in the denominator of Eq. (5) by a constant (or spatially dependent) k_0, while the model of Refs. 16 and 17 replaces all the ks with a constant. Equation (6) is similar to the gradient-driven closure used in Ref. 21, though they use the approximation $\partial_m q_{ijm} \propto \nabla^2(P_{ij} - p\delta_{ij})$, where p is the local isotropic pressure. The main differences are the explicit form of the heat-flux tensor, and the use of temperature gradients rather than gradients of the deviation from isotropy. Our approximation is closer to that of Ref. 25 extended to multiple dimensions. We also note that $\partial_m q_{ijm}$ is not traceless and there is no explicit relaxation to isotropy in the closure used here, unlike earlier models which use the isotropization as an approximation,[16,21] or a heuristic isotropization term to account for electron-scale instabilities.[43,44]

The moment equations coupled to Maxwell's equations are implemented in the finite-volume module of Gkeyll, which uses a high-resolution wave propagation method for the hyperbolic part of the equations and a local implicit method for the source terms.[14,45,46] The parabolic source term is evolved using a supertime-stepping method.[47]

III. RECONNECTION

A. Simulation set-up

We perform two-fluid ten-moment simulations of the island coalescence problem to study the effect of the closure described above. The initial conditions are a Fadeev equilibrium,[48] described by

$$\begin{aligned} A_y &= -\lambda B_0 \ln\left[\cosh(z/\lambda) + \epsilon\cos(x/\lambda)\right], \\ n &= n_0(1-\epsilon^2)/\left[\cosh(z/\lambda) + \epsilon\cos(x/\lambda)\right]^2 + n_b. \end{aligned} \tag{7}$$

Here, B_0 is the x-component of the magnetic field upstream of the layer, ϵ controls the island size, and λ is the half width of the current sheet. We use the same physical parameters as described in previous studies,[17,29,30] with $\epsilon = 0.4$, which corresponds to an island half-width of approximately 1.2λ, and background density $n_b = 0.2n_0$. The simulations are translationally symmetric in the y direction and the system size is $L_x \times L_z = 4\pi\lambda \times 2\pi\lambda$, with periodic boundary conditions in the x direction. Conducting walls for fields and reflecting walls for fluid quantities (and particles in the comparison kinetic simulations) are used in the z direction. For $\lambda/d_i = 5$, we use 640×320 cells, and maintain the same grid-spacing for larger systems. We use mass ratio $m_i/m_e = 25$, electron thermal speed $v_{t,e}/c = 0.35$, and $T_i = T_e = T$,

Published under license by AIP Publishing

and the value of T is set by the upstream equilibrium condition $\beta = 1$. The ratio of electron plasma frequency to gyrofrequency is $\omega_{pe}/\Omega_{ce} = 2$. A 10% initial perturbation in the magnetic field is applied to initiate merging in the center of the domain. The closure parameter for each species is set as $k_{0,s} = 1/d_s$, where d_s is the species inertial length. The reference kinetic results in this study were performed using VPIC[49] and PSC.[50]

In this geometry, the initial islands are unstable to the coalescence instability[51] and approach each other, causing a reconnecting current sheet to form in the center of the domain. The peak reconnection rate is reached around $t = t_A$, one global Alfvèn time of the system. We define the reconnection rate as $E_R = (1/B'V'_A)\partial\psi/\partial t$ in the same manner as Refs. 17, 29, and 30, where B' and V'_A are calculated using the maximum in-plane magnetic field between the centers of the two islands at $t = 0$. The flux within an island ψ is defined as the difference between A_y at the X- and O-points.

B. Reconnection rate

We first compare the reconnection rates using the ten-moment model to the results of kinetic simulations with varying system size and guide fields. The results are shown in Fig. 1, which compares the average reconnection rates (over $1.5t_A$) found in a Hall-MHD, two-fluid, and kinetic models. The use of the average rate rather than the peak rate is because reconnection in this system does not reach a steady-state. Similar comparisons have been performed in Refs. 17, 18, and 29. As mentioned earlier, the kinetic simulations showed a reduction of reconnection rate with system size. This was attributed to ion kinetic effects,[29] and was only reproduced in smaller systems when using the local and nonlocal ten-moment closures,[17,18] though the work of Ref. 21 did reproduce the kinetic scaling. When using the closure in Eq. (5), we obtain good agreement between the kinetic and ten-moment results at larger systems as well.

With the addition of a guide field, reconnection rates in kinetic simulations tend to return to Hall-MHD like values as the guide field increases.[52] This was attributed to a combination of a narrower ion-diffusion region and a reduction in the effects of the non-gyrotropic ion pressure tensor. As shown in Fig. 2, the maximum rate increases with the guide field up to $B_g/B_0 = 1$, before decreasing at a higher guide field, consistent with the rates obtained in kinetic simulations and fluid simulations using the local closure. As noted in Ref. 52, this behavior differs from the expectations of guide-field reconnection in symmetric current sheets, in which the reconnnection rate decreases for larger B_g. A similar trend is observed for the average reconnection rates.

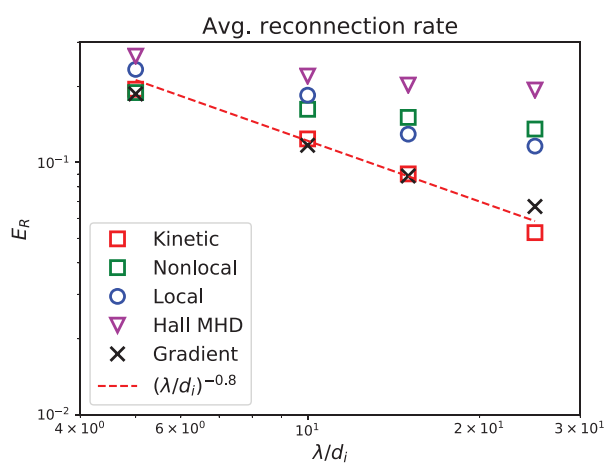

FIG. 1. Variation of average reconnection rates with system size for $B_g = 0$ using kinetic, Hall-MHD, and ten-moment models with local, nonlocal, and gradient-driven closures. The line shows the $(\lambda/d_i)^{-0.8}$ scaling found in Ref. 29.

C. Ion pressure tensor

In the fully kinetic and hybrid studies of island coalescence,[29,52] it was shown that for comparable T_i and T_e, a broad (2–3 d_i) ion diffusion region develops. Within this region, the non-ideal electric field is balanced by the divergence of the ion pressure tensor, in contrast to Hall MHD, where the ion inertia and resistivity balance the electric field in a narrower diffusion region. This was accompanied by ion anisotropy and agyrotropy, and the reduced reconnection rates were thus attributed to ion kinetic effects.

When using the ten-moment model, it was shown[17,18] that in small systems ($d_i/L = 5$), the wider ion diffusion region could be reproduced by modifying the free parameter in the ion pressure relaxation or by using the nonlocal closure. In Fig. 3, we present the decomposition of the ion momentum equation in the out-of-plane direction for simulations with $\lambda/d_i = 5$ and varying guide field. Using the temperature-gradient driven closure, when $B_g = 0$, the spatial extent of the non-ideal electric field shows that the wider ion diffusion region is still observed, and the ion pressure tensor is responsible for balancing the electric field. As B_g increases, the diffusion region becomes narrower, and the relative contribution of the inertial term becomes larger. These results are consistent with the earlier kinetic studies.[29,52]

The importance of the ion pressure tensor is also highlighted by using another common metric, the agyrotropy $A\varnothing$, which measures the deviation of the distribution function from cylindrical symmetry.[53] This quantity is shown in Fig. 4. In Ref. 18, it was shown that the nonlocal closure was able to reproduce the features of the ion agyrotropy found in kinetic simulations, while the model using local relaxation had qualitative discrepancies. In Fig. 4, we compare the structure of the ion agyrotropy in the fluid and kinetic simulations. When using the temperature-gradient driven closure, the features of the ion agyrotropy in the reconnection region are reproduced, with enhancement

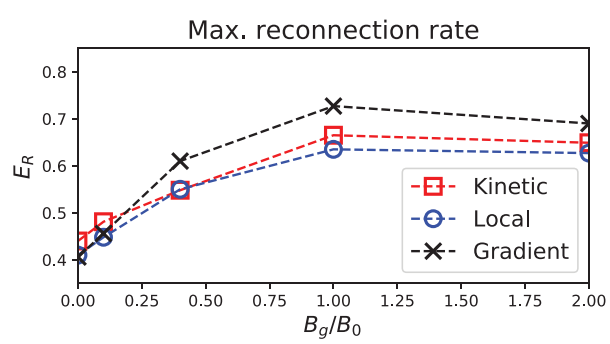

FIG. 2. Variation of maximum reconnection rates with guide field for $\lambda/d_i = 5$ using the gradient-driven closure. The local and kinetic rates are from Ref. 52.

Published under license by AIP Publishing

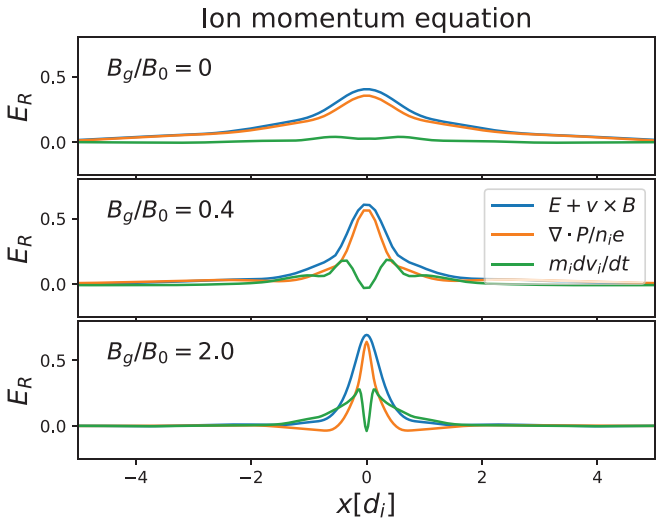

FIG. 3. Decomposition of the ion momentum equation showing the varying thickness and relative contributions of the ion inertia and pressure tensor at different values of the guide field. The $B_g = 2$ case used higher spatial resolution to resolve the electron gyroradius. This affected the peak value of $\nabla \cdot \mathbf{P}$ but not the maximum reconnection rate.

both upstream and downstream. This was previously only possible when using the nonlocal closure.[18] In contrast, the structure of the agyrotropy when using the local relaxation is qualitatively different, with little enhancement downstream and two distinct regions upstream.

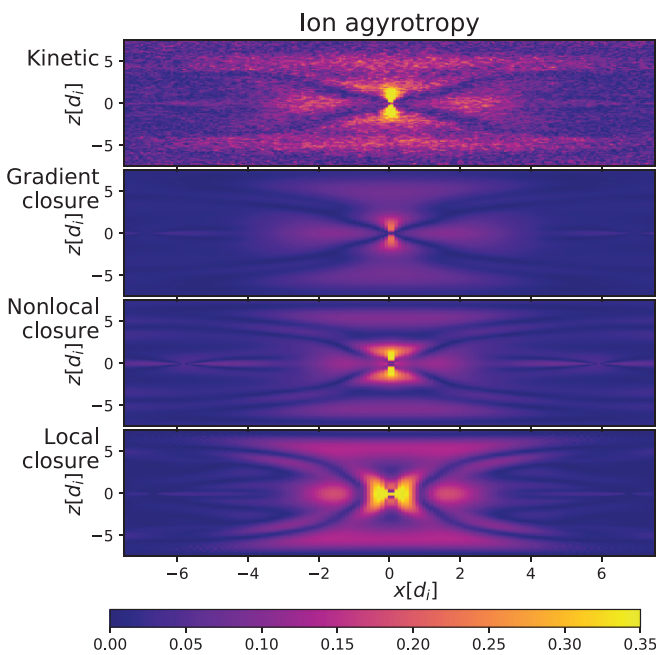

FIG. 4. Comparison of ion agyrotropy between kinetic and various ten-moment closures for $\lambda/d_i = 5$ and $B_g = 0$.

D. Electron pressure tensor

A weakness of the ten-moment closures used in Refs. 17 and 18 is the description of the electron dynamics. While the off diagonal components are sufficiently large to balance the reconnection electric field at the x-point in agreement with kinetic simulations,[16] the larger scale structure of the electron anisotropy is not reproduced. This is because the electrons are isotropized too strongly. When using the local isotropization, the relaxation rate of approximately $v_{t,e}/d_e$ is fast compared to the time scales of the system, while the closure used in Ref. 18 effectively allows too much heat-flux across field lines. As electron pressure anisotropy ($p_\parallel/p_\perp$) is important for setting the structure of reconnection regions,[54,55] it is important for the electron model to allow anisotropy to develop.

Figure 5 shows the electron pressure anisotropy from the $B_g = 0$, $\lambda/d_i = 5$ simulation using the various models. In the kinetic simulation, $p_\parallel$ is larger than $p_\perp$ in the region outside the two merging islands, but smaller than $p_\perp$ in the reconnection outflow. Electron anisotropy also develops outside the main island. As mentioned earlier, the electron pressure is almost isotropic when using local relaxation, aside from a small region around the x-point. The nonlocal closure shows some anisotropy but the values do not approach those found in the kinetic simulation.

There are still discrepancies between the fluid and kinetic model. There is no clear boundary between the main island and the outside regions at larger $|z|$, and there is no large $p_\parallel/p_\perp$ along the $z = 0$ line as can be seen in the kinetic simulations. The agreement can be improved by treating diffusion parallel and perpendicular to the magnetic field differently, as will be discussed in Sec. V.

IV. LOWER-HYBRID DRIFT INSTABILITY

In thin current sheets with density gradients, the lower-hybrid drift instability (LHDI) can be excited. This is an instability driven by

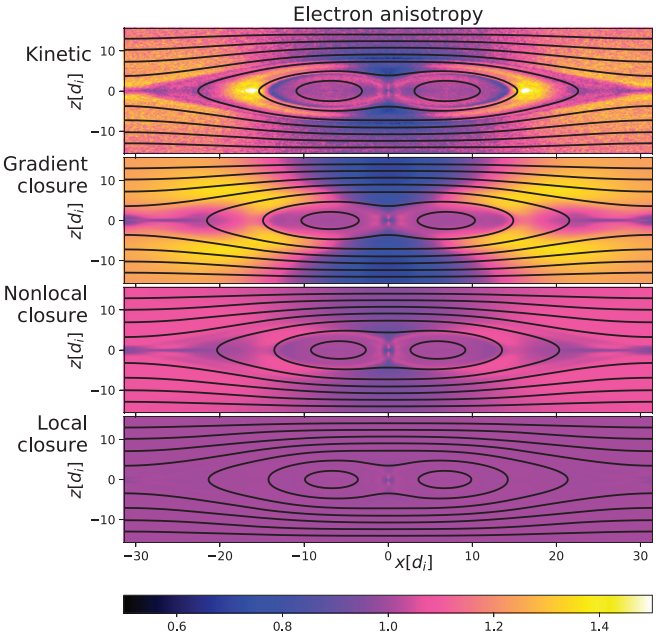

FIG. 5. Comparison of electron anisotropy between kinetic and various ten-moment closures.

Published under license by AIP Publishing

the diamagnetic current with a broad range of wavenumbers $(m_e/m_i)^{1/4} < k\rho_e < 1$ with frequency $\omega \approx \Omega_{lh} \sim \sqrt{\Omega_{ce}\Omega_{ci}}$.[31,56] The fluctuations are located at the edge of the current sheet, where the density gradient is the strongest, and have been observed in space, experiments, and simulations.[32,33,57]

We have shown previously in eigenmode calculations and simulations that the ten-moment model is able to capture the LHDI in the regime where the ion kinetic response is important when using a nonlocal heat-flux closure, while using the local relaxation of the pressure tensor led to parameter-dependent results.[19] In particular, using the same relaxation parameters as in reconnection simulations led to greatly reduced growth rates.

Here, we repeat the simulations performed in Ref. 19 to show the development of the LHDI using the gradient-driven closure. The initial conditions are a Harris sheet in the y-z plane, with $L = \rho_i$, $v_{t,e} = 0.06c$, $m_i/m_e = 36$, $T_i/T_e = 10$ with $L_y \times L_z = 6.4L \times 12.8L$. The simulations are given an initial perturbation with mode number 8, which corresponds to $k_y\rho_e \approx 0.41$. For these parameters, the kinetic ion response is important. We use both $k_s = 1/d_s$, which is used in reconnection simulations, and $k_s = k_y$ to show the effect of varying the effective conductivity parameter. The results are compared to the Vlasov–Maxwell simulations in Ref. 19.

The structure of the electric field E_y at $t\Omega_{ci} = 6$ is shown in Fig. 6, in which we compare the ten-moment results to the kinetic results of Ref. 19. The LHDI is excited in both fluid simulations away from the center of the current sheet, as expected for the electrostatic LHDI.[58] The measured growth rate with $k_s = k_y$ is $0.86\Omega_{ci}$, while with $k_s = 1/d_s$, the growth rate is $1.33\Omega_{ci}$. In the kinetic simulations of Ref. 19, the growth rate was $1.1\Omega_{ci}$, consistent with the growth rate from linear theory[31] in the most unstable region around $z/L = 1.6$. For comparison, the growth rate when using the local closure (with $k_{0,i} = k_y$, $k_{0,e} = 0$ as in Ref. 19) is $0.34\Omega_{ci}$, and the maximum E_y is an order of magnitude smaller at this time slice.

For the $k_s = k_y$ case, in which the free parameter is tuned to match the wavenumber of the excited mode, the structure of the LHDI

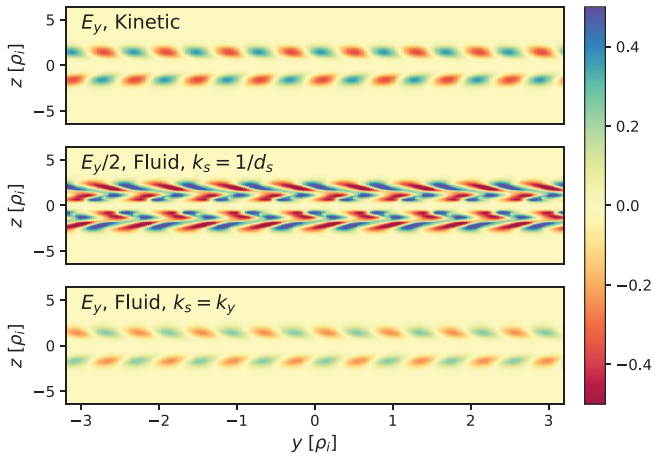

FIG. 6. Structure of E_y in simulations of the LHDI at $t\Omega_{ci} = 6$. E_y is normalized to $B_0 v_{A0}$. The electric field is reduced by a factor of two in the middle plot so the colors are not washed out as the growth rate is faster using the model with $k_s = 1/d_s$.

electric field is consistent with the kinetic result, and the slower growth rate is similar to that obtained when using the nonlocal closure[19] ($0.86\Omega_{ci}$ vs $0.84\Omega_{ci}$). When $k_s = 1/d_s$, the growth rate is faster, the mode structure has multiple peaks, and the LHDI electric field is stronger (we have reduced E_y by a factor of two in Fig. 6). Because of the faster growth rate, it is likely that other harmonics[58] have been excited and contribute to the electric field. We have confirmed this by looking at the electric field structure at earlier times, at which the mode structure is similar to the kinetic result.

These results show that it is possible to simulate both reconnection and the LHDI using the same parameters ($k_s \approx 1/d_s$), which was not possible with the local relaxation of the pressure tensor.[19,20] The role of the LHDI during the reconnection process is beyond the scope of this paper and will be the subject of future work. In kinetic simulations, it has been shown that the LHDI can increase the tearing mode growth rate prior to reconnection,[37,59] or lead to particle mixing[36] and cause apparent anomalous resistivity and viscosity.[35] It will thus be important to determine if the different growth rates obtained using the fluid model affect the physics of the reconnecting current sheet.

V. DISCUSSION

The use of a temperature-gradient-driven closure with the two-fluid ten-moment model shows marked improvements over previous approximations.[17,18] For reconnection in the island coalescence geometry, the reconnection rate shows a strong scaling with system size in agreement with kinetic simulations[29] and a different implementation of the gradient-driven closure.[21] In the case of guide-field reconnection, the variation of the reconnection rate is consistent with fully kinetic and hybrid studies,[52] as is the structure of the ion diffusion region. We have also been able to simulate the lower-hybrid drift instability in a current sheet with the ten-moment model, which was previously only possible when using a nonlocal closure or tuning the model parameters carefully.[19]

To date, the only large-scale simulations performed using the ten-moment model have used local relaxation of the pressure tensor,[20,22,23] with some success in comparison to observations. The closure used in this paper, while having larger computational costs, shows better agreement with kinetic simulations, particularly for the reconnection and instability physics being investigated.[20,22,23] An underlying reason behind the improvement is that the new closure can be understood as a relaxation of temperature to uniformity at a rate proportional to $k^2/|k_0|$ (in Fourier space) compared to a relaxation to isotropy with a fixed rate. This causes a lower relaxation rate at long wavelengths and a faster rate at short wavelengths, though the form differs from the $|k|v_t$ of Ref. 39 and there is a free parameter. It is interesting to note that the use of the closure in this paper gives better agreement with kinetic results than the full nonlocal version used in Ref. 18. This is because the implementation [Eq. (5)] is unmagnetized. The consequences of this can be seen in the better description of ion physics than electron physics as shown in Sec. III D since $\rho_i > \rho_e$, and the discrepancies at larger system sizes, where ρ_i becomes smaller compared to the system size. The effective $k^2/|k_0|$ scaling of the new closure reduces the contribution of longer wavelength perturbations to the heat flux, which is a better physical description. Further improvements to the model may include the modification of Eq. (6) so that the parallel and perpendicular heat-fluxes are treated separately. This will

Published under license by AIP Publishing

allow the perpendicular heat flux to be reduced in regions where the magnetic field is strong.

ACKNOWLEDGMENTS

This work was supported by DOE Contract No. DE-AC02–09CH11466, DOE Award No. DE-SC0016278, and NSF Grant No. AGS-1338944. We thank G. Hammett for many discussions about closures.

APPENDIX A: ROLE OF THE HEAT FLUX IN SYMMETRIC RECONNECTION

It was shown in Ref. 15 that the ten-moment model requires some kind of heat flux at the X-point to support reconnection in two dimensions. This has implications for the types of models that can be employed to capture reconnection. We reproduce the argument here in order to highlight the importance of the heat flux in higher-moment models and show that the naive addition of additional moments does not necessarily lead to better results.

Consider the equation for P_{xx} of either species at the X-point, where x is the outflow direction and z is the inflow direction,

$$\frac{\partial P_{xx}}{\partial t} + \nabla \cdot (\mathbf{u} P_{xx}) + 2(P_{xx}\partial_x u_x + P_{xz}\partial_z u_x) + \nabla \cdot \mathbf{q} = \frac{2q}{m}(B_z P_{xy} - B_y P_{xz}). \tag{A1}$$

In the steady state, consider the above equation along $x = 0$. By symmetry, $u_x = B_y = B_z = 0$, x gradients of P_{xx} and z gradients of u_x are zero. We find

$$u_z \partial_z P_{xx} + P_{xx} \nabla \cdot \mathbf{u} + 2P_{xx}\partial_x u_x + \nabla \cdot \mathbf{q} = 0. \tag{A2}$$

We can use the continuity equation to relate u_x and u_z. Along the z axis, we find

$$\partial_x u_x + \partial_z u_z = \frac{1}{n} u_z \partial_z n. \tag{A3}$$

Close to $z = 0$, we write $u_z = Cz^{2m+1} + O(z^{2m+2})$, $n = n_0 + Dz^{2l} + O(z^{2l+1})$ due to the symmetry of the reconnection region ($l \geq 1$, $m \geq 0$). Then from the continuity equation, the lowest order term on the RHS is z^{2l+2m}, while $\partial_z u_z = (2m+1)Cz^{2m} + O(z^{2m+1})$. Thus, $\partial_x u_x$ must be $-(2m+1)Cz^{2m}$ to leading order.

Substituting this back into the pressure equation (A2), we get

$$z\partial_z P_{xx} = 2(2m+1)P_{xx} + \frac{1}{Cz^{2m}} \nabla \cdot \mathbf{q}. \tag{A4}$$

If $\nabla \cdot \mathbf{q} = 0$, the differential equation has the solution

$$P = P_0 z^{2(2m+1)}, \tag{A5}$$

but this is zero at the origin, which is unphysical. This is illustrated in Fig. 7, which shows the electron pressure and out-of-plane momentum ρv_y in a ten-moment simulation of reconnection using the parameters of Ref. 60. The relaxation constant is zero for both species, while the geometry of the reconnection region is forming, the pressure at the center is becoming small, and the current sheet is unphysically split into four. Thus, there must be a heat flux or some collisional term to ensure a physical pressure at the X-point and allow reconnection to take place.

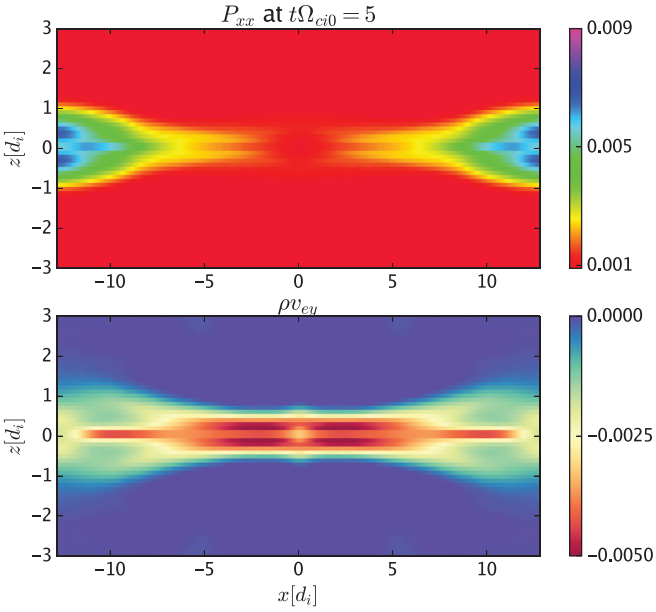

FIG. 7. Electron pressure P_{xx} and out-of-plane momentum density in a Harris sheet reconnection simulation with no pressure-tensor relaxation.

DATA AVAILABILITY

The data that support the findings of this study are available from the corresponding author upon reasonable request.

REFERENCES

[1] J. Raeder, J. Berchem, and M. Ashour-Abdalla, "The geospace environment modeling grand challenge: Results from a global geospace circulation model," J. Geophys. Res.: Space Phys. **103**, 14787–14797, https://doi.org/10.1029/98JA00014 (1998).

[2] G. Tóth, I. V. Sokolov, T. I. Gombosi, D. R. Chesney, C. R. Clauer, D. L. De Zeeuw, K. C. Hansen, K. J. Kane, W. B. Manchester, R. C. Oehmke, K. G. Powell, A. J. Ridley, I. I. Roussev, Q. F. Stout, O. Volberg, R. A. Wolf, S. Sazykin, A. Chan, B. Yu, and J. Kota, "Space weather modeling framework: A new tool for the space science community," J. Geophys. Res.: Space Phys. **110**, A12226, https://doi.org/10.1029/2005JA011126 (2005).

[3] P. Janhunen, M. Palmroth, T. Laitinen, I. Honkonen, L. Juusola, G. Facskó, and T. Pulkkinen, "The gumics-4 global MHD magnetosphere–ionosphere coupling simulation," J. Atmos. Sol.-Terr. Phys. **80**, 48–59 (2012).

[4] G. Chew, M. Goldberger, and F. Low, "The Boltzmann equation and the one-fluid hydromagnetic equations in the absence of particle collisions," Proc. R. Soc. London A **236**, 112–118 (1956).

[5] X. Meng, G. Toth, M. W. Liemohn, T. I. Gombosi, and A. Runov, "Pressure anisotropy in global magnetospheric simulations: A magnetohydrodynamics model," J. Geophys. Res.: Space Phys. **117**, A08216, https://doi.org/10.1029/2012JA017791 (2012).

[6] A. Otto, "Geospace environment modeling (GEM) magnetic reconnection challenge: Mhd and Hall MHD constant and current dependent resistivity models," J. Geophys. Res.: Space Phys. **106**, 3751–3757, https://doi.org/10.1029/1999JA001005 (2001).

[7] J. C. Dorelli, A. Glocer, G. Collinson, and G. Tóth, "The role of the hall effect in the global structure and dynamics of planetary magnetospheres: Ganymede as a case study," J. Geophys. Res.: Space Phys. **120**, 5377–5392, https://doi.org/10.1002/2014JA020951 (2015).

[8] Y. Kempf, D. Pokhotelov, S. von Alfthan, A. Vaivads, M. Palmroth, and H. E. J. Koskinen, "Wave dispersion in the hybrid-Vlasov model: Verification of Vlasiator," Phys. Plasmas **20**, 112114 (2013).

Published under license by AIP Publishing

[9]H. Karimabadi, H. X. Vu, D. Krauss-Varban, and Y. Omelchenko, "Global hybrid simulations of the earth's magnetosphere," in *Numerical Modeling of Space Plasma Flows*, Astronomical Society of the Pacific Conference Series, edited by G. P. Zank and N. V. Pogorelov (Astronomical Society of the Pacific, 2006), Vol. 359, p. 257.
[10]Y. Omelchenko and H. Karimabadi, "Hypers: A unidimensional asynchronous framework for multiscale hybrid simulations," J. Comput. Phys. **231**, 1766–1780 (2012).
[11]Y. Lin, J. R. Johnson, and X. Y. Wang, "Hybrid simulation of mode conversion at the magnetopause," J. Geophys. Res.: Space Phys. **115**, A04208, https://doi.org/10.1029/2009JA014524 (2010).
[12]G. Tóth, X. Jia, S. Markidis, I. B. Peng, Y. Chen, L. K. S. Daldorff, V. M. Tenishev, D. Borovikov, J. D. Haiducek, T. I. Gombosi, A. Glocer, and J. C. Dorelli, "Extended magnetohydrodynamics with embedded particle-in-cell simulation of ganymede's magnetosphere," J. Geophys. Res.: Space Phys. **121**, 1273–1293, https://doi.org/10.1002/2015JA021997 (2016).
[13]S. Lautenbach and R. Grauer, "Multiphysics simulations of collisionless plasmas," Front. Phys. **6**, 113 (2018).
[14]A. Hakim, "Extended MHD modelling with the ten-moment equations," J. Fusion Energy **27**, 36–43 (2008).
[15]E. A. Johnson, Ph.D. thesis, University of Wisconsin-Madison, 2011.
[16]L. Wang, A. H. Hakim, A. Bhattacharjee, and K. Germaschewski, "Comparison of multi-fluid moment models with particle-in-cell simulations of collisionless magnetic reconnection," Phys. Plasmas **22**, 012108 (2015).
[17]J. Ng, Y.-M. Huang, A. Hakim, A. Bhattacharjee, A. Stanier, W. Daughton, L. Wang, and K. Germaschewski, "The island coalescence problem: Scaling of reconnection in extended fluid models including higher-order moments," Phys. Plasmas **22**, 112104 (2015).
[18]J. Ng, A. Hakim, A. Bhattacharjee, A. Stanier, and W. Daughton, "Simulations of anti-parallel reconnection using a nonlocal heat flux closure," Phys. Plasmas **24**, 082112 (2017).
[19]J. Ng, A. Hakim, J. Juno, and A. Bhattacharjee, "Drift instabilities in thin current sheets using a two-fluid model with pressure tensor effects," J. Geophys. Res.: Space Phys. **124**, 3331–3346, https://doi.org/10.1029/2018JA026313 (2019).
[20]J. M. TenBarge, J. Ng, J. Juno, L. Wang, A. H. Hakim, and A. Bhattacharjee, "An extended MHD study of the 16 October 2015 MMS diffusion region crossing," J. Geophys. Res.: Space Phys. **124**, 8474–8487, https://doi.org/10.1029/2019JA026731 (2019).
[21]F. Allmann-Rahn, T. Trost, and R. Grauer, "Temperature gradient driven heat flux closure in fluid simulations of collisionless reconnection," J. Plasma Phys. **84**, 905840307 (2018).
[22]L. Wang, K. Germaschewski, A. Hakim, C. Dong, J. Raeder, and A. Bhattacharjee, "Electron physics in 3-d two-fluid 10-moment modeling of Ganymede's magnetosphere," J. Geophys. Res.: Space Phys. **123**, 2815–2830, https://doi.org/10.1002/2017JA024761 (2018).
[23]C. Dong, L. Wang, A. Hakim, A. Bhattacharjee, J. A. Slavin, G. A. DiBraccio, and K. Germaschewski, "Global ten-moment multifluid simulations of the solar wind interaction with mercury: From the planetary conducting core to the dynamic magnetosphere," Geophys. Res. Lett. **46**, 11584–11596, https://doi.org/10.1029/2019GL083180 (2019).
[24]S. Jarmak, E. Leonard, A. Akins, E. Dahl, D. Cremons, S. Cofield, A. Curtis, C. Dong, E. Dunham, B. Journaux, D. Murakami, W. Ng, M. Piquette, A. P. Girija, K. Rink, L. Schurmeier, N. Stein, N. Tallarida, M. Telus, L. Lowes, C. Budney, and K. Mitchell, "Quest: A new frontiers Uranus orbiter mission concept study," Acta Astronaut. **170**, 6–26 (2020).
[25]P. Sharma, G. W. Hammett, E. Quataert, and J. M. Stone, "Shearing box simulations of the MRI in a collisionless plasma," Astrophys. J. **637**, 952 (2006).
[26]X. Li, F. Guo, H. Li, and G. Li, "Particle acceleration during magnetic reconnection in a low-beta plasma," Astrophys. J. **843**, 21 (2017).
[27]M. Lyutikov, L. Sironi, S. S. Komissarov, and O. Porth, "Particle acceleration in relativistic magnetic flux-merging events," J. Plasma Phys. **83**, 635830602 (2017).
[28]M. Zhou, P. Bhat, N. F. Loureiro, and D. A. Uzdensky, "Magnetic island merger as a mechanism for inverse magnetic energy transfer," Phys. Rev. Res. **1**, 012004 (2019).
[29]A. Stanier, W. Daughton, L. Chacón, H. Karimabadi, J. Ng, Y.-M. Huang, A. Hakim, and A. Bhattacharjee, "Role of ion kinetic physics in the interaction of magnetic flux ropes," Phys. Rev. Lett. **115**, 175004 (2015).
[30]H. Karimabadi, J. Dorelli, V. Roytershteyn, W. Daughton, and L. Chacón, "Flux pileup in collisionless magnetic reconnection: Bursty interaction of large flux ropes," Phys. Rev. Lett. **107**, 025002 (2011).
[31]R. C. Davidson, N. T. Gladd, C. S. Wu, and J. D. Huba, "Effects of finite plasma beta on the lower-hybrid-drift instability," Phys. Fluids **20**, 301–310 (1977).
[32]S. D. Bale, F. S. Mozer, and T. Phan, "Observation of lower hybrid drift instability in the diffusion region at a reconnecting magnetopause," Geophys. Res. Lett. **29**, 33–1–33–4, https://doi.org/10.1029/2002GL016113 (2002).
[33]G. Lapenta, J. U. Brackbill, and W. S. Daughton, "The unexpected role of the lower hybrid drift instability in magnetic reconnection in three dimensions," Phys. Plasmas **10**, 1577–1587 (2003).
[34]D. B. Graham, Y. V. Khotyaintsev, C. Norgren, A. Vaivads, M. André, S. Toledo-Redondo, P.-A. Lindqvist, G. Marklund, R. Ergun, W. Paterson *et al.*, "Lower hybrid waves in the ion diffusion and magnetospheric inflow regions," J. Geophys. Res.: Space Phys. **122**, 517–533, https://doi.org/10.1002/2016JA023572 (2017).
[35]L. Price, M. Swisdak, J. F. Drake, P. A. Cassak, J. T. Dahlin, and R. E. Ergun, "The effects of turbulence on three-dimensional magnetic reconnection at the magnetopause," Geophys. Res. Lett. **43**, 6020–6027, https://doi.org/10.1002/2016GL069578 (2016).
[36]A. Le, W. Daughton, L.-J. Chen, and J. Egedal, "Enhanced electron mixing and heating in 3-d asymmetric reconnection at the earth's magnetopause," Geophys. Res. Lett. **44**, 2096–2104, https://doi.org/10.1002/2017GL072522 (2017).
[37]P. Ricci, J. U. Brackbill, W. Daughton, and G. Lapenta, "Influence of the lower hybrid drift instability on the onset of magnetic reconnection," Phys. Plasmas **11**, 4489–4500 (2004).
[38]K. G. Tanaka, I. Shinohara, and M. Fujimoto, "Parameter dependence of quick magnetic reconnection triggering: A survey study using two-dimensional simulations," J. Geophys. Res.: Space Phys. **111**, A11S18, https://doi.org/10.1029/2006JA011968 (2006).
[39]G. W. Hammett and F. W. Perkins, "Fluid moment models for landau damping with application to the ion-temperature-gradient instability," Phys. Rev. Lett. **64**, 3019–3022 (1990).
[40]G. W. Hammett, W. Dorland, and F. W. Perkins, "Fluid models of phase mixing, landau damping, and nonlinear gyrokinetic dynamics," Phys. Fluids B **4**, 2052–2061 (1992).
[41]P. B. Snyder and G. W. Hammett, "A landau fluid model for electromagnetic plasma microturbulence," Phys. Plasmas **8**, 3199–3216 (2001).
[42]P. J. Palmadesso, S. B. Ganguli, and H. G. Mitchell, "Multimoment fluid simulations of transport processes in the auroral zones," in *Modeling Magnetospheric Plasma* (American Geophysical Union, 1988), pp. 133–143.
[43]M. Hesse, D. Winske, and M. M. Kuznetsova, "Hybrid modeling of collisionless reconnection in two-dimensional current sheets: Simulations," J. Geophys. Res.: Space Phys. **100**, 21815–21825, https://doi.org/10.1029/95JA01559 (1995).
[44]L. Yin, D. Winske, S. P. Gary, and J. Birn, "Hybrid and Hall-MHD simulations of collisionless reconnection: Dynamics of the electron pressure tensor," J. Geophys. Res.: Space Phys. **106**, 10761–10775, https://doi.org/10.1029/2000JA000398 (2001).
[45]A. Hakim, J. Loverich, and U. Shumlak, "A high resolution wave propagation scheme for ideal two-fluid plasma equations," J. Comput. Phys. **219**, 418–442 (2006).
[46]L. Wang, A. Hakim, J. Ng, C. Dong, and K. Germaschewski, "Exact and locally implicit source term solvers for multifluid-maxwell systems," J. Comput. Phys. **415**, 109510 (2020).
[47]C. D. Meyer, D. S. Balsara, and T. D. Aslam, "A stabilized rungekuttalegendre method for explicit super-time-stepping of parabolic and mixed equations," J. Comput. Phys. **257**, 594 (2014).
[48]V. M. Fadeev, I. F. Kvartskhava, and N. N. Komarov, "Self-focusing of local plasma currents," Nucl. Fusion **5**, 202 (1965).
[49]K. J. Bowers, B. J. Albright, L. Yin, B. Bergen, and T. J. T. Kwan, "Ultrahigh performance three-dimensional electromagnetic relativistic kinetic plasma simulation," Phys. Plasmas **15**, 055703 (2008).

Published under license by AIP Publishing

[50]K. Germaschewski, W. Fox, S. Abbott, N. Ahmadi, K. Maynard, L. Wang, H. Ruhl, and A. Bhattacharjee, "The plasma simulation code: A modern particle-in-cell code with patch-based load-balancing," J. Comput. Phys. **318**, 305–326 (2016).
[51]J. M. Finn and P. K. Kaw, "Coalescence instability of magnetic islands," Phys. Fluids **20**, 72–78 (1977).
[52]A. Stanier, W. Daughton, A. N. Simakov, L. Chacón, A. Le, H. Karimabadi, J. Ng, and A. Bhattacharjee, "The role of guide field in magnetic reconnection driven by island coalescence," Phys. Plasmas **24**, 022124 (2017).
[53]J. Scudder and W. Daughton, "Illuminating electron diffusion regions of collisionless magnetic reconnection using electron agyrotropy," J. Geophys. Res.: Space Phys. **113**, a06222, https://doi.org/10.1029/2008JA013035 (2008).
[54]A. Le, J. Egedal, O. Ohia, W. Daughton, H. Karimabadi, and V. S. Lukin, "Regimes of the electron diffusion region in magnetic reconnection," Phys. Rev. Lett. **110**, 135004 (2013).
[55]J. Egedal, A. Le, and W. Daughton, "A review of pressure anisotropy caused by electron trapping in collisionless plasma, and its implications for magnetic reconnection," Phys. Plasmas **20**, 061201 (2013).
[56]W. Daughton, "The unstable eigenmodes of a neutral sheet," Phys. Plasmas **6**, 1329–1343 (1999).
[57]T. A. Carter, M. Yamada, H. Ji, R. M. Kulsrud, and F. Trintchouk, "Experimental study of lower-hybrid drift turbulence in a reconnecting current sheet," Phys. Plasmas **9**, 3272–3288 (2002).
[58]W. Daughton, "Electromagnetic properties of the lower-hybrid drift instability in a thin current sheet," Phys. Plasmas **10**, 3103–3119 (2003).
[59]W. Daughton, G. Lapenta, and P. Ricci, "Nonlinear evolution of the lower-hybrid drift instability in a current sheet," Phys. Rev. Lett. **93**, 105004 (2004).
[60]J. Birn, J. F. Drake, M. A. Shay, B. N. Rogers, R. E. Denton, M. Hesse, M. Kuznetsova, Z. W. Ma, A. Bhattacharjee, A. Otto, and P. L. Pritchett, "Geospace environmental modeling (GEM) magnetic reconnection challenge," J. Geophys. Res.: Space Phys. **106**, 3715–3719, https://doi.org/10.1029/1999JA900449 (2001).

Published under license by AIP Publishing